ISSN (e): 2250 – 3005 || Volume, 08 || Issue, 5|| May – 2018 ||

International Journal of Computational Engineering Research (IJCER)

Calibration of Infrared Thermometer Position for Control to Bead Geometry

Joon-Sik Son[1], Min-Ho Park[2], Tae-Jong Yun[1], Ji-Yeon Shim[3] And Ill-Soo Kim[2]

[1] *Research Institute of Medium& Small Shipbuilding 1703-8 Yongang-ri, Samho-eup, Yeongam, Jeonnam, 526-897, South Korea,*

[2] *Department of Mechanical Engineering, Mokpo National University, 1666 Youngsan-ro, Chungkye-myun, Muan-gun, Jeonnam, 534-729, South Korea,*

[3] *Convergence Components & Agricultural Machinery Application Center, KITECH, Palbok-dong 2-ga, Deokjin-du, Jeonju-city, Jeollabuk-do, 561-202, South Korea.*

Corresponding Author: Joon-Sik Son

ABSTRACT

Recently the demand to increase productivity and quality, the shortage of skilled labour and strict health and safety requirements finally led to the development of the robotic welding process to deal with many of the present problems of the welded fabrication. To make effective use of the robotic GMA(Gas Metal Arc) welding process, algorithm for sensing and controlling should be developed to give a high degree of confidence in predicting the bead dimensions and shape to accomplish the desired mechanical properties of the weldment. In addition, the arc travel in all directions must be accomplished within the range of the equipment and adjustments to the welding parameters. In this study, an infrared thermometer was employed to detect temperature distributions in the vicinity of the weld zone and to determine the optimal distance between welding wire and three infrared thermometers which applied for the automatic welding system. The optimal distance is used to the surface temperatures measured using infrared thermometers with the welding parameters (welding current, arc voltage) to be applicable for the real-time prediction of bead geometry. Comparison with values of coefficient of multiple correlations for curvilinear equation presents no differences, which indicate that the developed equations are reasonably suitable.

KEYWORDS: Infrared Sensor, Arc Welding Process, Welding Parameters, Bead Geometry, Temperature Distribution

---

Date of Submission: 18-04-2018 Date of acceptance: 03-05-2018

I. INTRODUCTION

1. Introduction

Welding quality can be achieved by the meeting of the quality requirements such as bead geometry and porosity inclusions and controlled by sensing either directly or indirectly the various welding parameters involved in the arc welding process. However, a fully adequate process control systems have not been developed due to a lack of reliable sensors and mathematical models that correlate welding parameters to the bead geometry for the automated arc welding process. In addition, the manipulator must also be suitable for carrying out weave patterns and meeting various demands such as positional accuracy, repeatability and travel speed [1]. Nevertheless, the completed fixtures which would ensure repeatability of component placement, adequate welding process would not be secured [2]. Therefore a robotic welding system, capable of detecting and making up for such variations in the working surroundings, must consider joint tracking and welding sensing.

A sensor that converts one type of physical quantity into another type, is probably the most important part in the robotic welding system. Weld pool size, shape and temperature distribution are examples of characteristics that direct sensor would monitor. Also this sensor monitors the final stage in the process from which information can be fed back to compensate for variations. Commercially available joint tracking systems incorporate both joint guidance and height control [3]. These systems assure that the welding arc will stay in the root of the joint and maintain an optimum stand-off distance. The systems are however limited by the quantity and quality of information that can be obtained from the arc signal [4]. Remwick and Richardson [5] employed arc sensing to

sense the GTA(Gas Tungsten Arc) pool motion and proposed the concept of weld pool motion as a bead geometry sensing technique. This concept is based on the fluid dynamics of the constrained weld pools, which depend on the properties of the molten pool material, the surface tension and the shape of weld pools [6]. Another application of arc sensing is the detection of the metal transfer in the GMA welding process. Johnson et al. [7] has attempted to correlate perturbations in the electrical arc signals with droplet transfer in order to detect the detachment of individual droplet and to distinguish the three transfer modes.

Infrared sensing, inherent attraction for the welding process, has had successful applications for the automated weld control. Also, infrared thermography is capable of monitoring the plate temperature distribution, which provides information for seam tracking, identification of plate geometry faults, penetration control, contamination and micro structure formation. Typical output parameters which have been investigated are cooling rate, discontinuity sensing, depth of penetration, contamination, seam tracking and bead geometry [8]. Ramsey et al. [9] investigated infrared thermography as a means of monitoring radiation, which is a function of both temperature and emissivity on the surface of aluminium weldment in close proximity to the welding arc. Infrared thermography was also employed by Lukens and Morris [10] to evaluate the weld metal cooling rates and to correlate the infrared emission intensity measurements to temperature using embedded thermocouples. Experimental results showed that the surface emissivity of the material would have a considerable effect on temperature.

Chin et al. [11] used the infrared thermography for sensing the arc welding process and monitored temperature distribution of the weld pool surface in order to detect variations in the welded part. They concluded that decreasing the welding current by 1/3 from the value required for bead penetration led to a decrease by 1/4 in both bead penetration and radius of the measured isotherm on the surface. Chen and Chin [12] related the surface temperature distribution to the depth of joint penetration and bead width, then compared the metallographic measurement of depth of penetration and bead width with the magnitude and gradients of the thermal profile. Nagarajan et al. [13] have reported on the application of infrared thermography to real-time for monitoring weld process. Weld depth of penetration control was obtained through monitoring the minor axis and ellipse isotherms which were shown to be the most sensitive variables to study the change due to variations into joint penetration depth and thickness of the plate being welded.

With the combination of sensors and mathematical models, increased effectiveness in control of the automatic welding process was achieved. Through-the-arc sensing has been applied from width control and seam tracking [14], to sensing of the GTA welding weld pool motion [15] and detection of the GMA welding metal transfer models [7]. Vision sensing has been utilized for joint tracking [16] and control of electrode extension. Other forms of sensing include infrared, which has been used in the estimation of penetration [17] as well as seam tracking [18], and ultrasonic sensing which has been applied to weld bead monitoring and inspection [19]. Although scanning infrared sensors are by far the most extensively used infrared for monitoring and controlling of the welding process, several intrinsic properties of these sensors have limited their practical industrial application. The infrared cameras are expensive, fragile in the harsh welding environment and require constant cooling using liquid nitrogen. Compared to infrared scanning cameras, infrared thermometers are inexpensive, rugged, and because of their compactness, can be placed close to welding arc.

In this study, an infrared thermometer was employed to detect temperature distributions in the vicinity of the weld zone. Therefore, infrared thermometer test should be performed for determining the optimal distance between welding wire and three infrared thermometers which applied for a real-time welding system. The objective of this study is to propose a new algorithm that provided the weld final configuration and properties as output and employed the process parameters as input. To achieve the objective, an empirical model involving the use of a multiple regression methods in robotic arc welding process have been developed to find a relationship between process parameters and thermal image from infrared thermography, and to investigate the interrelationship between isotherm radii versus bead width.

II. EXPERIMENTAL WORK

Fig. 1 shows a schematic diagram for the welding parameters and quality characteristics for experiment. Fig. 2 shows a schematic diagram for a distance between wire and infrared thermometers. Table 1 shows an experimental layout for calibration of infrared thermometer. Welding parameters for calibration were chosen the upper and lower limit of design of matrix. D1, D2 and D3 mean a distance of three infrared thermometers from welding torch.

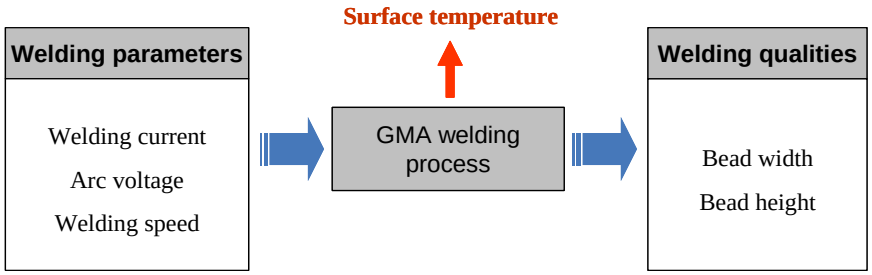

Figure 1. Schematic diagram for the welding parameters and quality characteristics for experiment

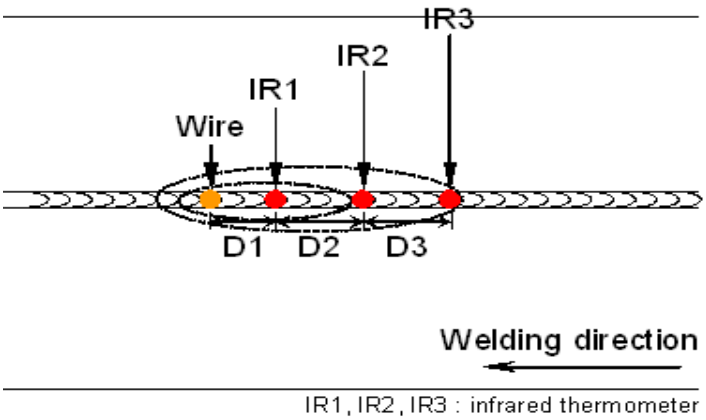

Figure 2. Schematic diagram for setup distance of infrared thermometers

Table 1. Experimental layout for calibration of infrared thermometer

Trial No.	C	V	S	D1	D2	D3
1	240	26	12	7	12	23
2	260	28	10	7	12	23
3	280	30	8	7	12	23
4	240	26	12	9	16	33
5	260	29	10	9	16	33
6	280	30	8	9	16	33

In this study, experiment was carried out on the base materials 300×150×4.5mm SS400 plates with bead-on-plate weld. In order to obtain good welding quality, the oxide scale in the interface was removed firstly by stainless wire brush and sand paper (#300). The selection of the electrode wire should be based principally upon matching the mechanical properties and physical characteristics of the base metal. Secondary consideration should be given to items such as the equipment to be used, the weld size and existing electrode inventory. 1.2Ø flux-cored wire diameters and 100% CO_2 shielding gas was employed in experiment.

Three infrared thermometers were employed to detect temperature in the vicinity of the weld pool and to determine the optical distance between welding wire and three infrared thermometers which employed for robotic welding system. A constant sensor position relative to the welding arc must be maintained during the GMA welding process. A sensor attachment was constructed for easy adjustment of the sensor position relative to the weld centerline. This attachment ensured a constant sensor-to-plate surface distance was maintained even in the case of distorted plates and allowed the sensor to travel along the welding direction. To keep low-frequency, high-power electric noise from the welding power source from infiltrating the infrared thermometer signal line used optical fiber tube. Fig. 3 shows the block diagram for control system on GMA welding process. The welding facility was chosen for the data collection and evaluation, Equipment to measure the distributions of the weld surface temperature was included infrared thermometers, arc monitoring system and desktop computer. A GMA welding unit employed in the experiment work is consisted of a robot control unit and a robot tech box. The torch positioning and motion control were achieved through monitoring the welding torch. With the welder and CO_2 shielding gas turned on, the robot was initialized and welding was then executed.

The shielding gas composition was Ar 80%+CO_2 20%. Experimental test plates were located in the fixture jig by the robot and the required weld conditions were fed for the particular weld steps in the robot path. With power supply and argon shield gas turned on, the robot was initialized and welding was executed. The bead geometry after welding was cut transversely from the middle position using wire cutting machine to measure the

bead width, and the incised specimen polished. A 3D scanner was used to measure precise the bead width. After scanned data of bead width, it was fitted by using commercial software called MALTAB.

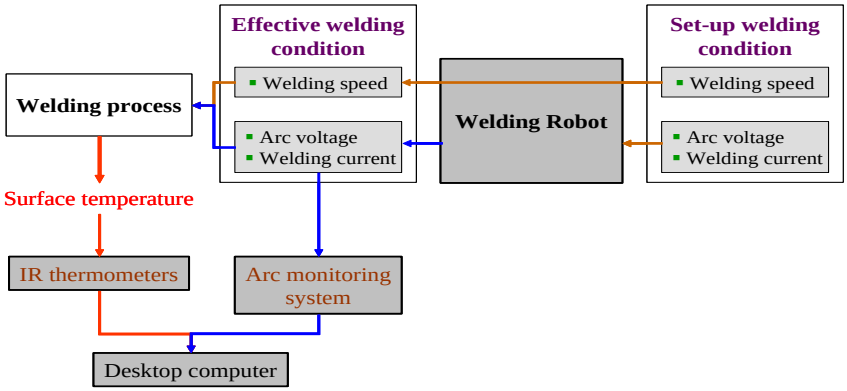

Figure 3. Block diagram for experimental setup

III. RESULTS AND DISCUSSION

3.1. Measurement of Bead Geometry

As rapid temperature fluctuations about a true mean value can make the thermometer output unsuitable for recording and control, the average function was employed to provide a smoothed signal in this experiment. The data acquisition system was employed for measurement of temperature distributions. It consisted of a desktop computer, LabVIEW data acquisition card and output module. The output signals were controlling current signals from infrared thermometer. A Virtual Instruments(VI) controller was constructed to facilitate the control of welding parameters from the computer screen. With the acquisition system combined with the VI, not only the program could be obtained the acquired data, but also output data were graphically displayed in real-time and could be saved into ASCII format for future analysis.

Fig. 4 represents the bead geometry measured at the middle position for GMA welding process. Fig. 5 proved the measured bead geometry using 3D scanner for calibration experiments. Also Fig. 6 indicated variations of the measured surface temperature for bead geometry using three infrared thermometers. It was shown that the highest temperature distributions was measured at offset distance between welding torch and 1st infrared thermometer (D1), while the lower temperature variations observed at offset distance between 2nd and 3rd infrared thermometer (D3). Besides, change of temperature fluctuation was increased as offset distance increased. As shown in Fig. 6(d)-(e), temperatures were not measured at 33 mm offset distances exactly. In case that the welding speeds is high speed, surface temperature distributions reduce fast so that the measured temperature is unstable at great distance from welding torch.

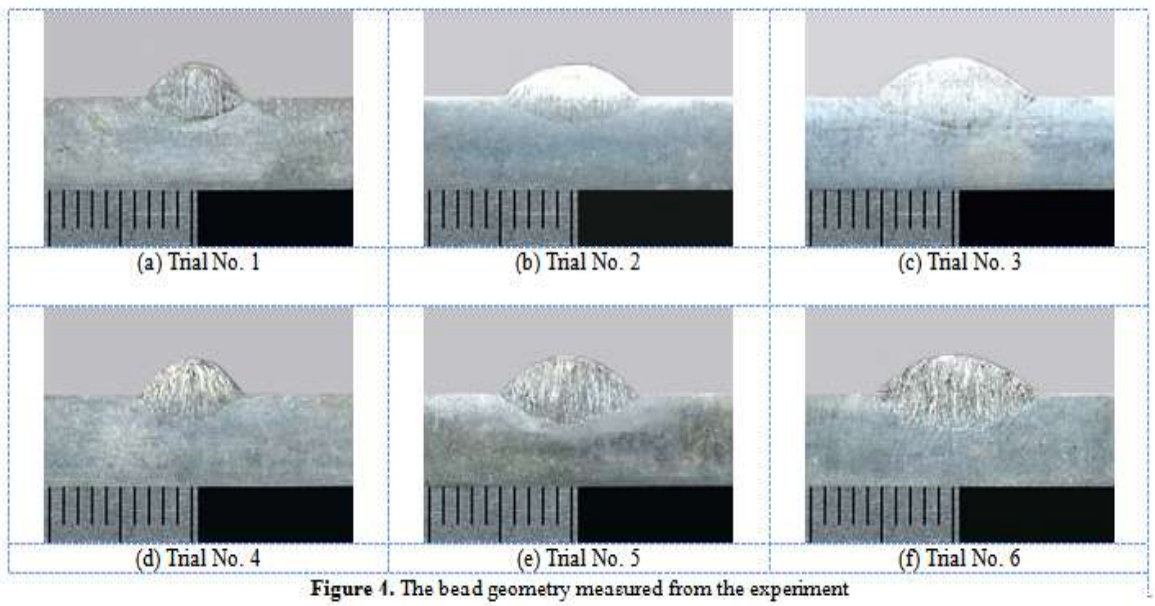

Figure 4. The bead geometry measured from the experiment

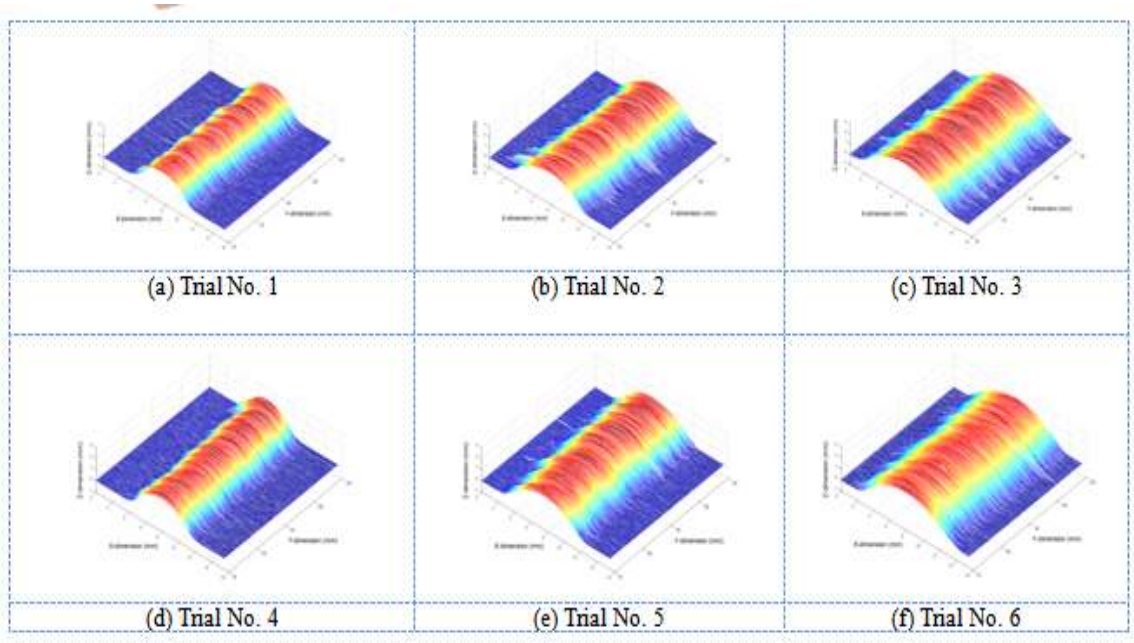

Figure 5. The measured bead geometry using 3D scanner in calibration experiment

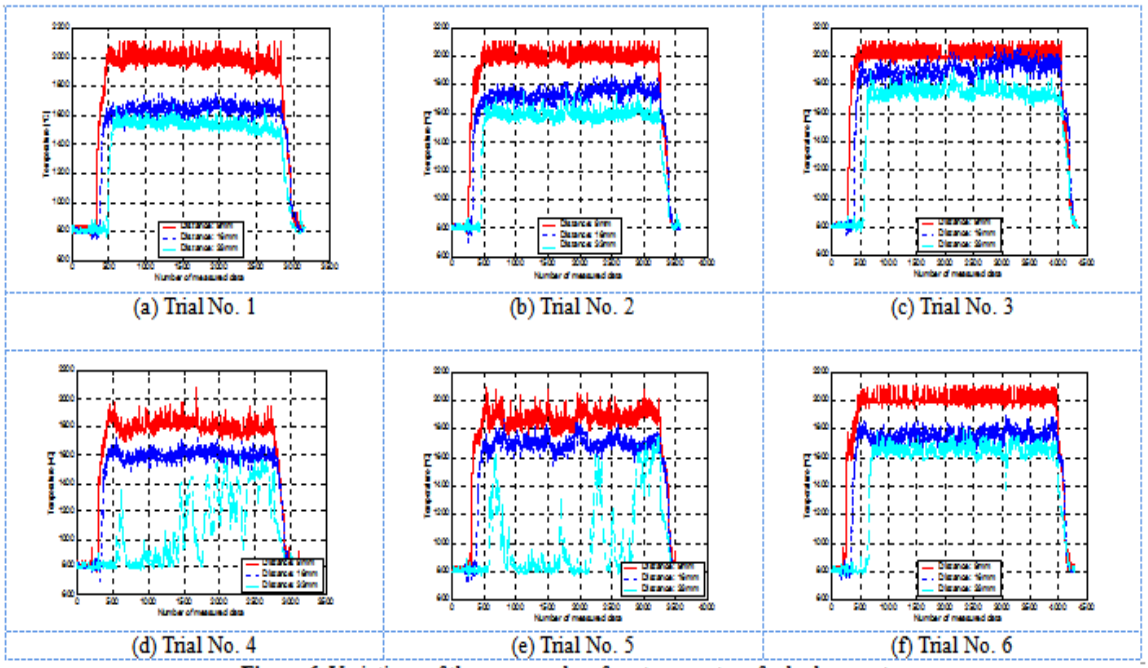

Figure 6. Variations of the measured surface temperature for bed geometry

3.2. Optimization of Infrared Thermometer Position

In order to determine of optimal offset distance between welding torch and infrared thermometers, the mathematical models to study relationship between the measured temperature distributions and bead width have been developed. The response function can be represented as follow;

$$Y = f(T) \quad (1)$$

In which, $\boldsymbol{Y}$ is the measured bed width, $\boldsymbol{T}$ the measured temperature distributions.

For the analysis of correlation, it was used the Standard Error of Estimate($\boldsymbol{SEE}$), coefficient of correlation($\boldsymbol{R}$) and coefficient of determination ($\boldsymbol{R}^2$). Where $\boldsymbol{SEE}$ is used to identify an accuracy of the estimated values, $\boldsymbol{R}$ is the value to represent correlation between temperature distributions and bead width, $\boldsymbol{R}^2$ is a coefficient to represent an accuracy of regression equation. $\boldsymbol{SEE}$, $\boldsymbol{R}$ and $\boldsymbol{R}^2$ can be represented as follow;

$$SEE = \frac{\sigma}{\sqrt{N}} \quad (2)$$

$$R = \sqrt{\frac{SSR}{SST}} \quad (3)$$

$$R^2 = \frac{SSR}{SST} \quad (4)$$

Where σ is standard deviation, ***N*** is the number of data, Sum of Squared Regression(***SSR***) is quantity that afactor expresses a depended variable as sum of square for factor, $SSR = \sum(x_i - \bar{x})$, Sum of Squared Total (***SST***) is quantity that total plus Sum of Squared Error (***SSE***) and ***SSE*** is quantity that a cause excluded factors, expresses a depended variable.

In order to use that a values has a good correlation between temperature distributions and bead width, mean temperature distributions has been compared as the same way that distance analyzed. Table 2 demonstrates the results of analysis for correlation between temperature distributions and bead width. Usually, in case $\boldsymbol{R}^2 > 0.65$, regression model can be considered good correlation between factor and depended variable. ***R*** expresses between factor and depended variable. As shown in Table 2, temperature distributions at 9mm had a good correlation with quantity of correlation bead width more than temperature variations at 7mm so that the optimal value was the minimum value in D1. In case D2, temperature distributions at 12mm and 16mm had similar correlation with bead width, but $\boldsymbol{R}^2$ of temperature distributions at 12mm for bead width was higher than that of 0.65. Temperature variations at 33mm in D3 had not correlation with bead width because $\boldsymbol{R}^2$ values for 33mm was smaller than 0.65. Temperature distributions at 23mm in D3 was that minimum value is shown best value. To compare performance of the models, the target was evaluated by PAM(Predictive Ability of Model) defined by Poliak et al. [20] as expressed in the following equation;

$$PAM = \frac{N_{pam}}{N_{total}} \times 100 \quad (5)$$

Where N_{pam} is the predicted value of range $\left|\frac{B_m - B_p}{B_m}\right| \le 0.1$ and N_{total} is the entire predicted values.

Table 2. The regression analysis results of temperature for bead width

Symbol	Distance(mm)	Temperature Characteristics	***R***	$\boldsymbol{R}^2$	Standard Error of Estimate
D1	7	Mean	0.553	0.306	1.56403
	9	Mean	0.859	0.738	0.89157
D2	12	Mean	0.931	0.868	0.68332
	16	Mean	0.881	0.776	0.82462
D3	23	Mean	0.908	0.824	0.78793
	33	Mean	0.696	0.484	1.25195

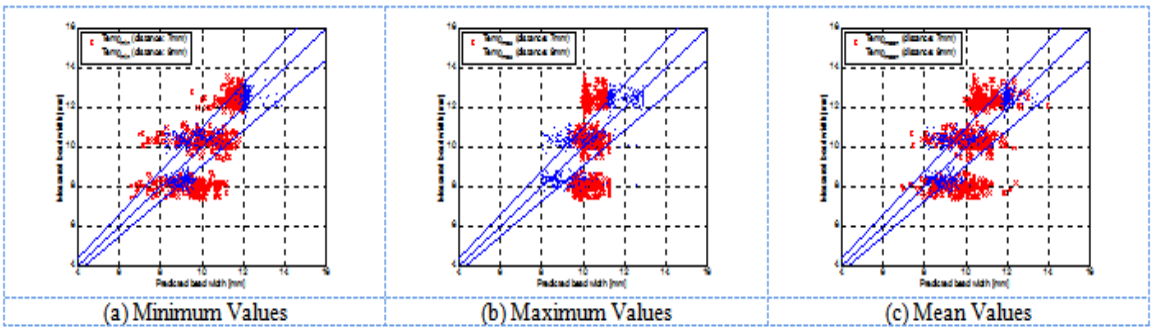

(a) Minimum Values (b) Maximum Values (c) Mean Values

Figure 7. Comparison of the predicted and measured bead width at D1

Figs. 7-8 show correlation between temperature distributions and bead width at D1. In Figs. 7-8, the solid line represents the best fit, and the dotted line means over 90% PAM. Temperature distributions have good correlation with bead width when the predicted values are distributed concentrically to solid line. Fig. 7 proves comparison of the predicted and measured bead width at D1. As shown in Fig. 7, temperature variations at 9mm are concentrated more than that at 7mm. Maximum temperature variations do not express bead with as shown in Fig. 7(b). The error of predicted bead width at D1 represents Fig. 8. This was used in order to identify performance of predicted equation through analysis of distribution of error. It was shown that temperature distributions at 9mm presented more accuracy than that at 7mm for bead width. Table 3 indicates PAM and standard deviation. As shown in Table 3, temperature at 9mm appeared a good agreement more than that at 7mm for bead geometry. In PAM, it cannot select optimal values from maximum, minimum and mean values. Therefore we searched the temperature distributions with the least values in standard deviation and chosen minimum value at 9mm.

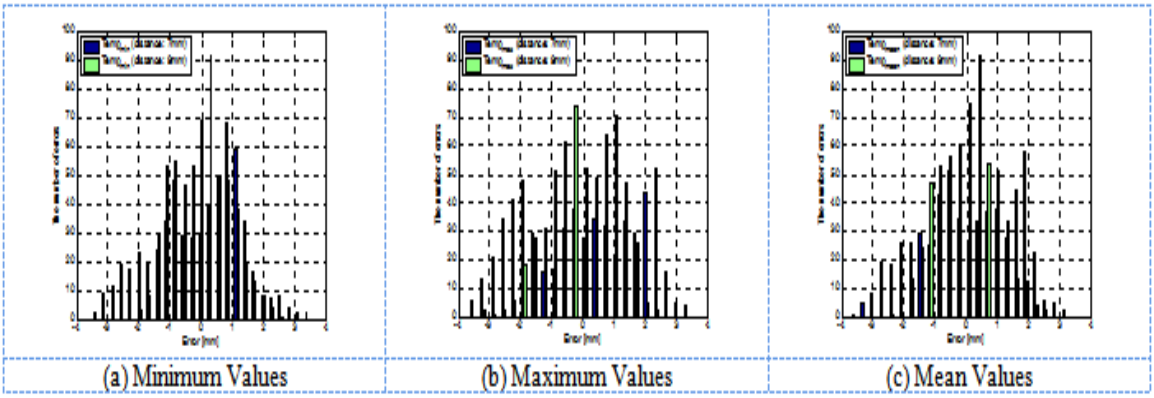

(a) Minimum Values (b) Maximum Values (c) Mean Values

Figure 8. The error of the predicted bead width for at D1

Table 3. Analysis results for D1 point

Bead Geometry	Distance(mm)	Temperature Characteristics	PAM	Standard Deviation
Bead Width	7	Minimum	54.8223	1.3893
		Maximum	32.8257	1.8195
		Mean	42.3012	1.5627
	9	Minimum	67.0051	0.8871
		Maximum	65.1438	1.0466
		Mean	69.2047	0.8953

In order to determine optimal point of infrared thermometer at D2, correlation between temperature distributions and bead width was represented in Figs. 9-10. As shown in Figs. 9-10, both temperature distributions at 12mm and 16mm had a good correlation with bead width, because relationship between temperature distributions and bead width is linear mostly. And because all kinds of temperature without classification by distance and data processing had a similar correlation with bead width, searching of optimal point was very difficult. The results shown in Table 4 ware the same. Therefore, in order to determine optimal point of infrared thermometer at D2, several facts should be considered. First, 12mm of infrared thermometer from welding torch is so close to D1 because the optimal point of infrared thermometer at D1 is 9mm and measurement diameter of infrared thermometer is 5mm. Secondly, at 12mm of infrared thermometer from welding torch is smaller than 0.65 as shown in Table 4. Therefore, 16mm as the optimal point of infrared thermometer at D2 was determined.

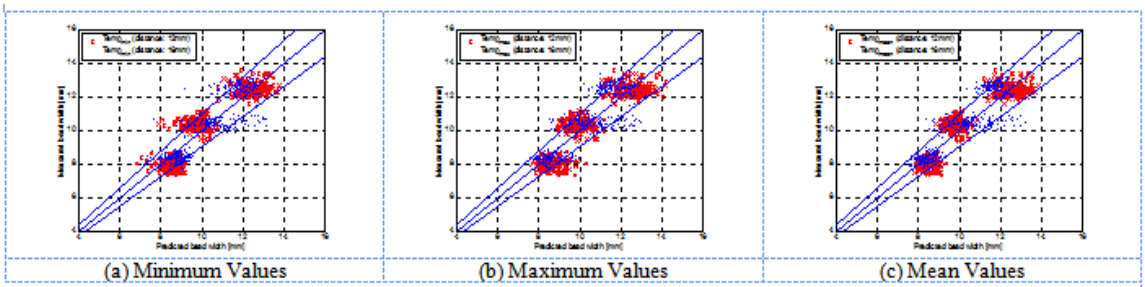

(a) Minimum Values (b) Maximum Values (c) Mean Values

Figure 9. Comparison of the predicted and measured bead width at D2

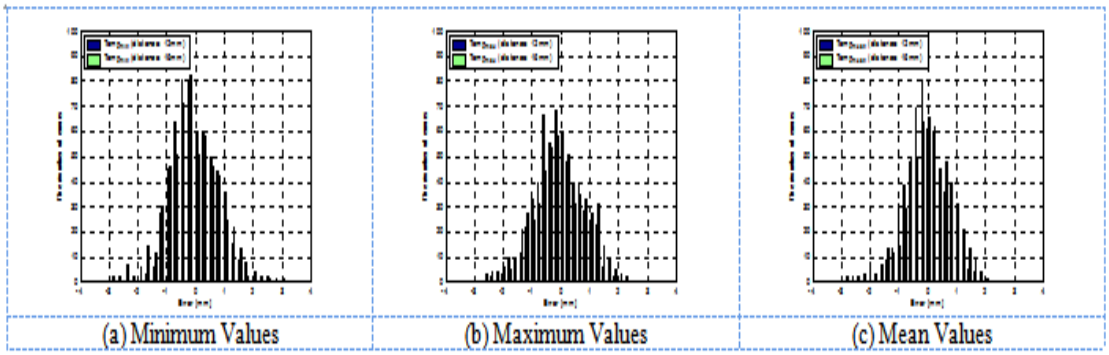

Figure 10. The error of the predicted bead width for at D2

Table 4. Analysis results for D2 point

Bead Geometry	Distance(mm)	Temperature Characteristics	PAM	Standard Deviation
Bead Width	12	Minimum	81.2183	0.7415
		Maximum	79.3570	0.7682
		Mean	84.0948	0.6827
	16	Minimum	73.9425	0.8974
		Maximum	73.0964	0.9204
		Mean	81.2183	0.8213

Figs. 11-12 represent correlation between temperature distributions at D3 and bead width. As shown in Figs. 11-12, distributions of predicted bead width are presented like a perpendicular line which, means that temperature variations at 33mm didn't predict bead width according to a change of welding condition. Distribution of error at 23mm is closer to 0 than that of a 33mm as shown in Figs. 11-12. Table 5 represents that selection of the minimum temperature for prediction of bead width had a better performance than those of minimum and mean temperature distributions. Therefore, it should be concluded that optimization is minimum temperature at 23mm. From the previous analysis results, the offset distance for D1, D2 and D3 on main experiment used is determined 9, 16 and 23mm respectively.

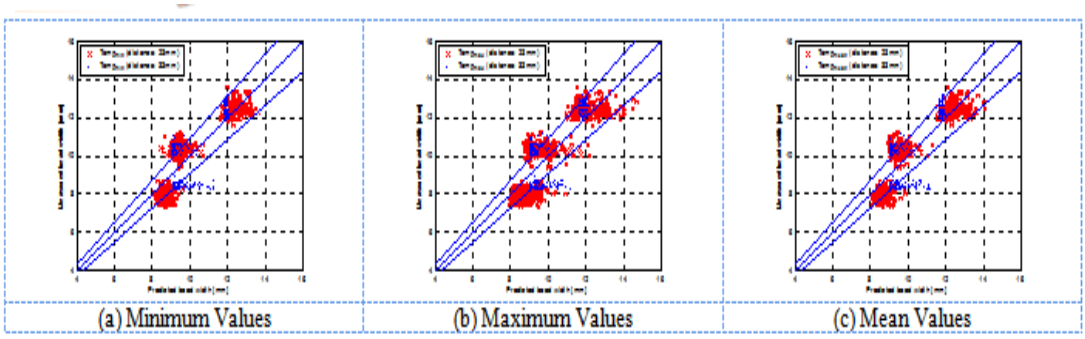

Figure 11. Comparison of the predicted and measured bead width at D3

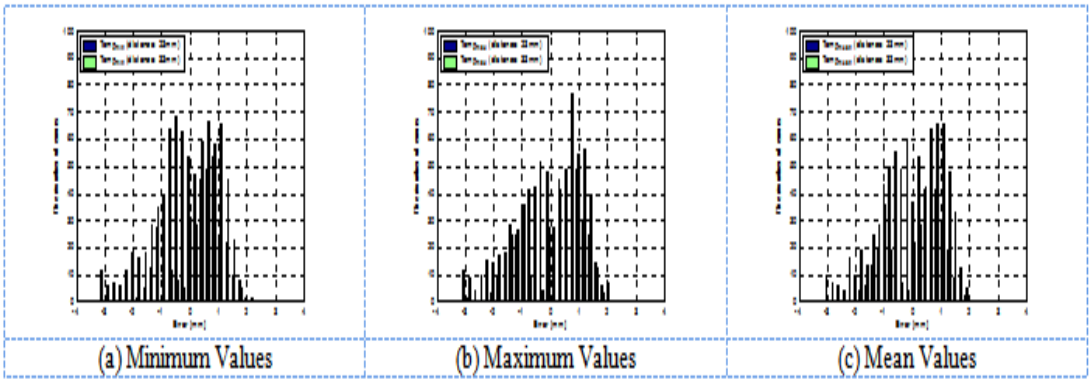

Figure 12. The error of the predicted bead width for at D3

Table 5. Analysis results for D3 point

Bead Geometry	Distance(mm)	Temperature Characteristics	PAM	Standard Deviation
Bead Width	23	Minimum	77.8342	0.7721
		Maximum	66.4975	0.9565
		Mean	74.7885	0.7873
	33	Minimum	48.7310	1.2475
		Maximum	49.2386	1.2593
		Mean	47.5465	1.2578

IV. CONCLUSION

The algorithm to determine optimal point of infrared thermometer and to investigate the correlation between temperature distributions and bead width for the GMA welding process has been developed, and the following conclusions reached:

1. Bead-on-plate welding was conducted on 6 specimens with a change of welding parameters such as welding current, arc voltage and welding speed to detect temperature distributions in vicinity of weld zone. Surface distributions of the base materials were measured using three infrared thermometers to determine a setup distance from welding torch. The highest temperature distributions was measured at offset distance between welding torch and 1st infrared thermometer (D1), while the lower temperature variations observed at offset distance between 2nd and 3rd infrared thermometer (D3). In addition, the welding speed is increased, surface temperature distributions reduce fast so that the measured temperature is unstable at great distance from welding torch.
2. The new algorithm to study relationship between the measured temperature distributions and bead width to determine of optimal offset distance between welding torch and infrared thermometer have been developed. Temperature distributions at 9mm had a good correlation with bead width more than temperature variations at 7mm in D1. Also, temperature distributions at 12mm and 16mm in case D2 had similar correlation with bead width. Temperature distributions at 23mm in D3 was that minimum value is shown best value.
3. PAM(Predictive Ability of Model) to verify the performance of the developed algorithms was employed. Both temperature distributions at 12mm and 16mm at D2 had a good correlation with bead width. Offset distance for D1, D2 and D3 from the developed algorithm is determined 9, 16 and 23mm respectively. The algorithm for the optimal distance between welding wire and three infrared thermometers may be achieved with the development of appropriate computer interface with the technique used for infrared thermography.

ACKNOWLEDGEMENT

This research was supported by Basic Science Research Program through the National Research Foundation of Korea (NRF) funded by the Ministry of Education (No.2015R1D1A 3A01020246).

REFERENCES

[1] R. K. Miller, Industrial robot hand book. SEIA Technical Publications, 153-158, 1987.
[2] S. J. Marburger, Welding automation and computer control. Welding : Theory and Practices, Elsevier Science Publishers, B. V., 209-233, 1990.
[3] J. E. Agapakis, J. M. Katz, M. Koifman, G. N. Epstein, J. M. Friedman, D. O. Eyring & H. J. Rutishauser, Joint tracking and adaptive robotic welding using vision sensing of the weld joint geometry. Welding Journal, 65(11), 33-41, 1986.
[4] R. W. Richardson, A. Gutow, R. A. Anderson & D. F. Farson, Coaxial weld pool viewing for process monitoring and control. Welding Journal, 63(3), 43-50, 1984.
[5] R. J. Remwick & R. W. Richardson, Experimental investigation of GTA weld pool oscillation. Welding Journal, 62(2), 29-35, 1983.
[6] D. E. Hardt, Measuring weld pool geometry from pool dynamics. Modeling and Control of Casting and Welding Processes : Proceedings of the 3rd Conference on Modeling of Casting and Welding Processes, Santa Barbara, California, USA, 12-17, 1986.
[7] J. A. Johnson, N. M. Carlson & H. B. Smartt, Detection of metal trasfer mode in GMAW. Recent Trends in Welding Science and Technology : TWR `89 : Proceedings of the 2nd International Conference on Trends in Welding Research, Gatlinburg, Tennessee, USA, 14-18, May, 337-181, 1989.
[8] J. P. Boillet, P. Cielo, G. Begin, C. Michel, M. Lessard, P. Fafard & D. Villemure, Adaptive welding by instrumental considerations. Welding Journal, 64(7), 209-217, 1985.
[9] P. W. Ramsey, J. J. Chyle, J. N. Kuhr, P. S. Myers, M. Weiss & W. Froth, Infrared temperature sensing system for automatic fusion welding. Welding Journal, 42(8), 337-346, 1963.
[10] W. E. Lukens & R. A. Morris, Infrared temperature sensing of cooling rates for arc welding control. Welding Journal, 61(1), 27-33, 1982.
[11] B. A. Chin, N. H. Madsen & J. S. Goodling, Infrared thermography for sensing the arc welding process. Welding Journal, 62(9), 227-234, 1983.
[12] W. Chen & B. A. Chin, Monitoring joint penetration using infrared sensing techniques. Welding Journal, 69(4), 181-185, 1990.
[13] S. Nagarajan, K. N. Groom & B. A. Chin, Infrared sensors for seam tracking is gas tungsten arc welding processes. Recent Trends in Welding Science and Technology: TWR `89 : Proceedings of the 2nd International Conference on Trends in Welding Research, Gatlinburg, Tennessee, USA, 14-18, May, 951-955, 1989.
[14] G. E. Cook, Though-the-arc sensing for arc welding. Proceedings of the 10th Conference on Production Research and Technology, National Science Foundation, March, 141-151, 1983.

[15] R. W. Richardson, Robotic weld joint tracking systems - Theory and implementation methods. Welding Journal, 65(11), 43-51, 1986.
[16] P. M. Gonseth & P. Blanc, Optiguide - A new optical joint tracking device. Welding Journal, 62(9), 27-29, 1983.
[17] R. J. Salter & R. T. Deam, A practical front face penetration control system for TIG welding. Developments in Automated and Robotic Welding. Cambridge, UK, The Welding Institute, 1-12, 1987.
[18] W. H. Chen, P. Banjerjee & B. A. Chin, Study of penetration variations in automated gas tungsten arc welding. Recent Trends in Welding Science and Technology : TWR `89 : Proceedings of the 2nd International Conference on Trends in Welding Research, Gatlinburg, Tennessee, USA, 14-18, May, 517-522, 1989.
[19] S. Nagarajan, W. H. Chen & B. A. Chin, Infrared sensing for adaptive arc welding. Welding Journal, 68(11), 462-466, 1989.
[20] E. I. Poliak, Application of linear regression analysis in accuracy assessment of rolling force calculations, Metals and Materials, 4(5), 1047-1056, 1998.

Joon-Sik Son "Calibration of Infrared Thermometer Position for Control to Bead GeometryInternational Journal of Computational Engineering Research (IJCER), vol. 08, no. 05, 2018, pp. 01-10.